

Johns Hopkins University
Johns Hopkins University, Dept. of Biostatistics Working Papers

Year 2007

Paper 139

A BAYESIAN HIERARCHICAL
FRAMEWORK FOR SPATIAL MODELING
OF fMRI DATA

F. DuBois Bowman* Brian S. Caffo†
Susan Spear Bassett‡ Clinton Kilts**

*Department of Biostatistics, The Rollins School of Public Health, dbowma3@sph.emory.edu

†Department of Biostatistics, The Johns Hopkins Bloomberg School of Public Health

‡Department of Psychiatry and Behavioral Sciences, Johns Hopkins Medical Institutions

**Department of Psychiatry and Behavioral Sciences, Emory University

This working paper is hosted by The Berkeley Electronic Press (bepress) and may not be commercially reproduced without the permission of the copyright holder.

<http://www.bepress.com/jhubiostat/paper139>

Copyright ©2007 by the authors.

A BAYESIAN HIERARCHICAL FRAMEWORK FOR SPATIAL MODELING OF fMRI DATA

F. DuBois Bowman, Brian S. Caffo, Susan Spear Bassett, and Clinton Kilts

Abstract

Functional neuroimaging techniques enable investigations into the neural basis of human cognition, emotions, and behaviors. In practice, applications of functional magnetic resonance imaging (fMRI) have provided novel insights into the neuropathophysiology of major psychiatric, neurological, and substance abuse disorders, as well as into the neural responses to their treatments. Modern activation studies often compare localized task-induced changes in brain activity between experimental groups. One may also extend voxel-level analyses by simultaneously considering the ensemble of voxels constituting an anatomically defined region of interest (ROI) or by considering means or quantiles of the ROI. In this work we present a Bayesian extension of voxel-level analyses that offers several notable benefits. First, it combines whole-brain voxel-by-voxel modeling and ROI analyses within a unified framework. Secondly, an unstructured variance/covariance for regional mean parameters allows for the study of inter-regional functional connectivity, provided enough subjects are available to allow for accurate estimation. Finally, an exchangeable correlation structure within regions allows for the consideration of intra-regional functional connectivity. We perform estimation for our model using Markov Chain Monte Carlo (MCMC) techniques implemented via Gibbs sampling which, despite the high throughput nature of the data, can be executed quickly (less than 30 minutes). We apply our Bayesian hierarchical model to two novel fMRI data sets: one considering inhibitory control in cocaine-dependent men and the second considering verbal memory in subjects at high risk for Alzheimer's disease. The unifying hierarchical model presented in this manuscript is shown to enhance the interpretation content of these data sets.

A Bayesian Hierarchical Framework for Spatial Modeling of fMRI Data

F DuBois Bowman*, Brian Caffo†, Susan Spear Bassett‡, Clinton Kilts§

April 12, 2007

Abstract

Functional neuroimaging techniques enable investigations into the neural basis of human cognition, emotions, and behaviors. In practice, applications of functional magnetic resonance imaging (fMRI) have provided novel insights into the neuropathophysiology of major psychiatric, neurological, and substance abuse disorders, as well as into the neural responses to their treatments. Modern activation studies often compare localized task-induced changes in brain activity between experimental groups. One may also extend voxel-level analyses by simultaneously considering the ensemble of voxels constituting an anatomically defined region of interest (ROI) or by considering means or quantiles of the ROI. In this work we present a Bayesian extension of voxel-level analyses that offers several notable benefits. First, it combines whole-brain voxel-by-voxel modeling and ROI analyses within a unified framework. Secondly, an unstructured variance/covariance for regional mean parameters allows for the study of inter-regional functional connectivity, provided enough subjects are available to allow for accurate estimation. Finally, an exchangeable correlation structure within regions allows for the consideration of intra-regional functional connectivity. We perform estimation for our model using Markov Chain Monte Carlo (MCMC) techniques implemented via Gibbs sampling which, despite the high throughput nature of the data, can be executed quickly (less than 30 minutes). We apply our Bayesian hierarchical model to two novel fMRI data sets: one considering inhibitory control

*Department of Biostatistics, The Rollins School of Public Health

†Department of Biostatistics, Johns Hopkins Bloomberg School of Public Health

‡Department of Psychiatry and Behavioral Sciences, Johns Hopkins Medical Institutions

§Department of Psychiatry and Behavioral Sciences, Emory University

in cocaine-dependent men and the second considering verbal memory in subjects at high risk for Alzheimer's disease. The unifying hierarchical model presented in this manuscript is shown to enhance the interpretation content of these data sets.

Key words and phrases: functional imaging, image analysis, MCMC, medical imaging, neuroimaging, regions of interest.

1 Introduction

Functional neuroimaging techniques enable *in vivo* investigations into the neural basis of human cognition, emotions, and behaviors. In practice, applications of functional magnetic resonance imaging (fMRI) have provided insights into the pathogenesis and pathophysiology of major psychiatric, neurologic, and substance abuse disorders, as well as into the neural responses to their treatments. We commonly employ fMRI to conduct *activation* studies and studies of *functional connectivity*, depending on the research objectives. Activation studies generally seek to characterize the magnitude and volume of neural responses to experimental tasks by detecting differences in patterns of brain activity between various experimental conditions, between different subgroups of subjects, and between two or more scanning sessions, e.g. before and after treatment. The objective of functional connectivity studies is to determine different areas of the brain that share similar temporal task-related (or resting-state) brain activity properties. Currently applied techniques consist of distinct statistical methodology for activation and functional connectivity studies. We develop a common statistical framework for activation and functional connectivity studies, and activation results from our approach account for prominent functional connections in the brain.

We develop a statistical modeling framework that builds on the two-stage approach commonly applied in activation studies for fMRI data. The conventional two-stage approach considers individualized models at the first stage and population- or group-level models at the second stage (Worsley et al., 2002), both fitting separate models at each voxel. The voxel-by-voxel analyses employ estimation techniques that assume an improbable lack of correlation between voxel pairs. However, there is emerging recognition of the importance of modeling spatial correlations between voxels both for estimation and for statistical inferences. Some investigators attempt to capture

correlations between the measured brain activity in a given voxel with the activity in neighboring voxels. For example, Katanoda et al. (2002) address spatial correlations by incorporating the time series from neighboring (physically contiguous) voxels. Similarly, Gössl et al. (2001) and Woolrich et al. (2004a) consider correlations between neighboring voxels using a conditional autoregressive (CAR) model in a Bayesian framework, and specifically Woolrich et al. (2004a) model correlations as a function of the geometric mean of the number of neighboring voxels. Penny et al. (2005) present a Bayesian model that assumes spatially correlated prior distributions for the regression coefficients. They consider first-order neighbors (possibly extendable) in their spatial model and assume that the covariance matrix is known up to a multiplicative constant by defining a known spatial kernel matrix and by specifying a prior gamma distribution for the unknown constant.

Other authors extend spatial modeling beyond a localized neighborhood by simplifying the structure of the data. For example, Worsley et al. (1991) present a quadratic decay spatial correlation model for PET data from a selected number of anatomical regions, rather than voxels, significantly reducing the data and the dimensions of the correlation matrix. In a loosely related application, Albert and McShane (1995) present a generalized estimating equations (GEE) approach for spatially correlated binary data from a study of brain lesions, with a relatively small number (e.g. 88) of spatial locations in each slice. Bowman (2007) considers data from a defined region of interest and presents a spatio-temporal model that specifies spatial correlations based on a functionally defined distance metric. In this model, the magnitude of correlations decay as a function of decreasing similarity, rather than simply as a function of increasing physical distance, allowing the possibility of long range correlations due, for example, to white-matter axonal connections.

Bowman (2005) presents a whole-brain spatio-temporal model that partitions voxels into functionally related networks and applies a spatial simultaneous autoregressive model to capture intra-regional correlations between voxels. A key practical advantage of this approach is that it leads to fast estimation. Woolrich et al. (2004b) propose a Bayesian modeling framework for fMRI data allowing both separable and nonseparable spatio-temporal models. As an alternative to modeling spatial correlations, one may indirectly address non-independence between voxels by initially smoothing the data, performing separate univariate analyses at each voxel, and then applying random field theory to determine statistical significance for the entire set of voxels, which makes

assumptions about spatial dependencies between voxels (Worsley et al., 1992; Worsley, 1994). The random field theory approach to hypothesis testing links voxel-wise statistics, generally by assuming a stationary or isotropic random field, but it does not directly estimate spatial covariances/correlations under a linear model. Holmes et al. (1996) outlines several issues with the random field approach, including low degrees of freedom to support the theory, noisy statistic images, a questionable assumption of constant error variance across an entire image, and initial spatial smoothing of the data.

The spatial modeling approaches of Katanoda et al. (2002), Gössl et al. (2001), and Woolrich et al. (2004a) provide local smoothing, but limiting spatial associations to a very restricted area (e.g. consisting of contiguous voxels) departs from our current knowledge regarding neurophysiology including functional networks that are spatially disperse (e.g. the visual system). Broca's area and Wernicke's area are specific examples of two noncontiguous anatomical regions that may exhibit long range correlations, given their joint involvement in many language related tasks (Matsumoto et al., 2004). Bowman (2007) demonstrates that a relatively distant pair of voxels may exhibit high positive correlations, even when compared to a more proximal pair of voxels. Local spatial models disregard the possibility of such long-range correlations. Although the approach of Penny et al. (2005) is capable of extending the localized region, it makes an assumption of a known local spatial kernel, rather than estimating all of the variances and spatial covariances from the data.

Considering a coarsened data structure, such as the methods of Worsley et al. (1991) and Albert and McShane (1995), simplifies computations, but sacrifices the potential for localization using fMRI (or PET) data. Bowman (2005) frames a spatial model within a simplified data structure by modeling intra-regional correlations. While this method may incorporate long-range spatial correlations and provides inferences at a refined voxel level as well as broader regional levels, it suffers from the assumption that inter-region voxel pairs are uncorrelated. In contrast to the computationally efficient method of Bowman (2005), the approaches by Woolrich et al. (2004a), Gössl et al. (2001), and Bowman (2007) require extensive computations. Consequently, these methods are less practical due to the long computation times or are limited to small or moderate anatomic regions. For example, Bowman (2007) only considers analyses for regions of interest,

such as the cerebellum, and the method of Woolrich et al. (2004a) takes roughly 6 hours to analyze data from a single slice.

In this paper, we develop a Bayesian hierarchical statistical model for spatially correlated neuroimaging data. Specifically, we develop a new spatial model for making inferences regarding task-related changes in brain activity, which identifies and accounts for prominent functional connections in the brain. Hierarchical models are general tools for estimating and making inferences about quantities that can be conceptualized through a multi-level process. The Bayesian hierarchical approach provides a viable alternative to classical statistical methods for fitting complex models because it divides the parameters across different stages of the model that can be estimated using Markov chain Monte Carlo (MCMC) methods. Bayesian methods offer inferential advantages by providing samples from the joint posterior probability distribution for all of the model parameters, rather than p-values, providing greater flexibility in the inferences that may be drawn from a functional neuroimaging study.

Below, we discuss the proposed Bayesian hierarchical model, estimation procedures, and applications of our model to experimental data from two fMRI studies. The main advantages that our proposed spatial model yields are that it: 1) provides a novel approach to uncover prominent functional connections between remote voxels, 2) often provides higher accuracy and increased statistical power for inferences regarding task-related changes in brain activity by adjusting for spatial associations in the data, 3) extends the modeling assumptions underlying previously applied methods from the limited amount of research in this area, and 4) establishes a unified framework that yields results for voxel-specific inferences, regional or VOI inferences, and functional connectivity.

2 Experimental fMRI data

2.1 Inhibitory control in cocaine-dependent men

Impairments in the ability to exert inhibitory control over drug-related behaviors, in spite of adverse consequences, represents a common characteristic of drug addictions (Kalivas and Volkow, 2005). These inhibitory control deficits exhibited by cocaine addicts can be modeled using response inhibition tasks outside of a drug seeking context. We consider an fMRI study that evaluates the

impact of cocaine addiction and treatment-related cocaine abstinence on neural representations of motor inhibition tasks targeting prepotent response inhibition.

Data are available for 15 cocaine-dependent men who have both pre- and post-treatment scans, with the follow-up scans occurring roughly 24 days following the initial image acquisitions and after completion of an intensive outpatient behavioral therapy program without relapse. Baseline and follow-up scans are also available for 17 control subjects, matched to the clinical sample on age, race, gender, handedness, education, and early life adversity. Within each session or treatment period, the data consist of serial fMRI scans on each person. Subjects received information about the procedures and risks of the study and provided written consent to participate in the study protocol approved by an Institutional Review Board.

Targeting inhibitory control processes, we consider scans corresponding to a Stop-signal task, designed to evaluate the ability to cancel a prepotent motor response (Aron and Poldrack, 2006). The task involves repeated presentations of visual Go stimuli (uppercase alphabetical letters), appearing for 500 milliseconds with an inter-stimulus interval of 2.3 sec. Subjects execute the speeded Go response by pressing a button as quickly as possible. A Stop signal, an auditory tone (at 1,000 Hz), lasting 500 milliseconds, occurs at random in 16% of the trials. The presentation of the Stop signal following the Go stimulus is an indicator to the subject to attempt to refrain from executing the Go response.

2.2 Alzheimer's disease

Alzheimer's disease is a debilitating degenerative disorder impacting millions of older adults in the United States alone (Brookmeyer et al., 1998). Currently there is no known cure, or effective treatments, for Alzheimer's disease. Since pathologic changes occur before the onset of clinical symptoms, pre-clinical differences in neurological function between eventual Alzheimer's cases and controls are of fundamental interest to early detection and intervention strategies. This observation is emphasized by the fact that the available treatments have greater clinical benefit the earlier they are introduced (see Tariot and Federoff, 2003, for example).

Bassett et al. (2006) demonstrated that fMRI activation patterns differ between subjects at high risk for Alzheimer's disease and group-matched controls in an auditory word-pair-associate

task. This task, developed by Bookheimer et al. (2000), was chosen for its role as a processing demand for the medial temporal lobe (MTL), as the MTL is often indicated as an early site of neuropathological changes associated with Alzheimer's disease . The auditory task consists of a memory "encode" phase, whereby subjects are presented unrelated word pairs in a block and a "recall" block, where subjects are asked to recall the second word of the pair when presented with the first. The paradigm consisted of two six minute sessions, each consisting of seven unique word-pairs.

Subjects were defined as at-risk for Alzheimer's disease by having an autopsy confirmed affected parent and at least one additional clinically diagnosed first degree relative. Both at-risk and control subjects were over 50 years of age and free of memory impairments at the time of the study. All subjects provided written consent and the study was approved by the Johns Hopkins Institutional Review board. The at-risk and control groups did not statistically differ on any key covariates. However, there was some degree of asymmetry in terms of the number of APOE $\epsilon 4$ alleles, which are a known marker for Alzheimer's disease, and gender, with a higher percentage of females in the at-risk group.

Using this paradigm and sample, Bassett et al. (2006) found changes in neural activation between the at-risk patients and the controls in the temporal lobe, including the frontal gyrii and right hippocampus. In this manuscript, we analyze a followup study on the same group of individuals using the same experimental paradigm. We focus only on comparison of the encode blocks to resting state. Notably, this study included nearly 100 subjects in each group, and limited the image acquisition to a small axial volume surrounding the MTL. As such, the study offers unique data for investigating functional connectivity between regions of interest.

3 A hierarchical model for functional neuroimaging data

We formulate a model that builds on the conventional two-stage modeling approach for fMRI data that emulates a random effects analysis. Our model captures temporal correlations via the random effects structure and by addressing serial dependencies between each subject's repeated measurements, e.g. assuming an autoregressive-type model (Worsley et al., 2002). We extend the con-

ventional approach by fitting a spatial Bayesian hierarchical model at the second stage, where we capture correlations between voxels within defined neuroanatomical structures as well as between different anatomical regions. Incorporating spatial correlations into our statistical model allows us to quantify and make inferences about functional connections between intra-regional voxels and between defined anatomical nodes (regions).

3.1 Stage I: general linear model with serially correlated errors

In light of our two fMRI data examples examining response inhibition among cocaine-dependent men and verbal memory for subjects at-risk for Alzheimer's disease, we present the Stage I model initially for an fMRI study. However, the general framework that we present is also applicable to PET regional cerebral blood flow (rCBF) studies, and one may consider a range of substantive applications that seek to identify localized regions of significant task-related (or between-group) changes in measured brain activity. The first-stage of our approach resembles a general linear model (GLM) for each individual's vector of serial responses at the voxel level (Friston et al., 1995). To set notation, let $i = 1, \dots, K_j$ index subjects, $s = 1, \dots, S$ represent scans, and $v = 1, \dots, V$ index voxels. We arrange the serial fMRI blood oxygenation-level dependent (BOLD) responses for subject i , measured at voxel v , in the $S \times 1$ vector $\mathbf{Y}_i(v)$. The $S \times q$ design matrix \mathbf{X}_{iv} includes independent variables of interests such as experimental conditions, and \mathbf{H}_{iv} contains covariates that are not of substantive interest, e.g. including a high-pass filtering matrix used to remove unwanted low-frequency trends from the data. For fMRI analyses, we convolve the design matrix with a prespecified hemodynamic response function.

We specify the first-stage model as follows:

$$\mathbf{Y}_i(v) = \mathbf{X}_{iv}\boldsymbol{\beta}_i(v) + \mathbf{H}_{iv}\boldsymbol{\nu}_i(v) + \boldsymbol{\epsilon}_i(v), \quad (1)$$

where $\boldsymbol{\beta}_i(v) = \{\beta_{i1}(v), \dots, \beta_{iq}(v)\}'$ and $\boldsymbol{\beta}_{ij}(v)$ is the effect corresponding to stimulus j (for subject i), $\boldsymbol{\nu}_i(v)$ includes parameters associated with \mathbf{H}_{iv} , and the mean-zero vectors of random errors $\boldsymbol{\epsilon}_i(v)$ are independent and follow a multivariate normal distribution with variance $\text{Var}\{\boldsymbol{\epsilon}_i(v)\} = \tau_v^2 \mathbf{I}$. To make the variance model assumption tenable, one may apply a pre-whitening transformation, e.g. based on a first-order autoregressive model, to address serial correlations between multiple scans.

3.2 Stage II: spatial Bayesian hierarchical model

We consider an anatomical parcellation of the brain consisting of $g = 1, \dots, G$ regions, where we may set G as high as 116 (Tzourio-Mazoyer et al., 2002). Alternative anatomical parcellations are also available, for instance, one based on defined Brodmann regions (Garey, 1994). Generally, we expect a fair degree of similarity of the fMRI time courses for voxels within a region. For region g , which contains V_g voxels, we denote the individualized Stage I estimate of the mean fMRI BOLD response vector associated with stimulus j by $\beta_{igj} = \{\beta_{igj}(1), \dots, \beta_{igj}(V_g)\}'$. These estimates result from applying a Stage I model analogous to that specified in Equation 1, with effects in the design matrices suitably defined to correspond to the experimental tasks. We also modify our earlier notation here by collecting localized effects from all voxels in region g into a single vector . Stage two of our analysis proposes a Bayesian hierarchical model that accounts for spatial correlations between intra-regional voxels and also between regions. In particular, our model has the following hierarchical structure:

$$\begin{aligned}
\beta_{igj} \mid \boldsymbol{\mu}_{gj}, \alpha_{igj}, \sigma_{gj}^{-2} &\sim \text{Normal}(\boldsymbol{\mu}_{gj} + \mathbf{1}\alpha_{igj}, \sigma_{gj}^2 \mathbf{I}) \\
\boldsymbol{\mu}_{gj} \mid \lambda_{gj}^2 &\sim \text{Normal}(\boldsymbol{\mu}_{0gj}, \lambda_{gj}^2 \mathbf{I}) \\
\sigma_{gj}^2 \mid \boldsymbol{\Gamma}_j &\sim \text{Gamma}(a_0, b_0) \\
\boldsymbol{\alpha}_{ij} \mid \boldsymbol{\Gamma}_j &\sim \text{Normal}(\mathbf{0}, \boldsymbol{\Gamma}_j) \\
\lambda_{gj}^{-2} &\sim \text{Gamma}(c_0, d_0) \\
\boldsymbol{\Gamma}_j^{-1} &\sim \text{Wishart}\left\{(h_0 \mathbf{H}_{0j})^{-1}, h_0\right\}
\end{aligned} \tag{2}$$

where $\boldsymbol{\mu}_{gj} = (\mu_{gj}(1), \dots, \mu_{gj}(V_g))'$ and $\boldsymbol{\alpha}_{ij} = (\alpha_{i1j}, \dots, \alpha_{iGj})'$.

The first level of our hierarchical model specifies a multivariate normal likelihood function for the response vectors, β_{igj} , containing each subject's mean BOLD activity from the experimental tasks of interest (from Stage I). For each voxel, $v = 1, \dots, V_g$, the subject-specific quantities $\beta_{igj}(v)$ are assumed to vary randomly about a mean consisting of both a population-level mean parameter $\mu_{gj}(v)$ and an individualized (random effect) component α_{igj} . Given the random effects parameter, α_{igj} , the covariance matrix of β_{igj} is given by $\sigma_{gj}^2 \mathbf{I}$. Our model yields a conditional independence assumption, indicating that the spatial correlations between all pairs of voxels within region g are

mediated by the random effects parameters.

At the next level, the model expresses a prior belief that each voxel's population mean, (for the j th effect), arises from a normal distribution with a mean given by the overall region mean, i.e. $\mu_{0gj}(v) = \mu_{0gj}$, for all voxels $v = 1, \dots, V$, plus mean-zero random error with variance λ_{gj}^2 . The data will help to inform this prior assumption, but it seems to represent a reasonable starting point to assume that voxels within anatomically-defined regions exhibit task-related activity that deviates around an overall mean for that region. At the final level, our hierarchical model captures potential functional connections between anatomical brain regions through the covariance matrix Γ_j . We provide additional details regarding functional connectivity below in Section 3.3.

In addition to voxel-specific quantities, interest may also lie in regional parameters that pool a collection of voxels in a region \mathcal{R}_g . From our model, it is natural to define regional parameters such as the mean regional activation: $\theta_{gj} = \sum_{v \in \mathcal{R}_g} \mu_{gj}(v)/V_g$. Another candidate would consider the upper percentiles of regional activation. We can easily estimate these regional parameters using samples from the joint posterior distribution for all of our model parameters, taking into account the potential correlations between voxel-specific parameters from the region. The first level of the hierarchical model in 2 can be conceived from the following linear model formulation

$$\beta_{igj} \mid \boldsymbol{\mu}_{gj} = \boldsymbol{\mu}_{gj} + \mathbf{1}\alpha_{igj} + \epsilon_{igj}, \quad (3)$$

where $\epsilon_{igj} \sim \text{Normal}(\mathbf{0}, \sigma_{gj}^2 \mathbf{I})$. Note that conditional on $\boldsymbol{\mu}_{gj}$, β_{igj} has an exchangeable covariance structure, based on this model expression. Specifically,

$$\text{Var}(\beta_{igj} \mid \boldsymbol{\mu}_{gj}) = \gamma_{gg}^{(j)} \mathbf{J} + \sigma_{gj}^2 \mathbf{I},$$

where $\gamma_{gg}^{(j)}$ is g th diagonal element from Γ_j , representing the regional variance. The exchangeable model builds in (equal) correlations between all pairs of voxels within a defined anatomical region.

3.3 Functional connectivity

Our Bayesian hierarchical model (2) allows us to capture information regarding the functional connectivity both within a defined anatomical structure and between brain regions. Friston et al. (1993) describes functional connectivity as the correlations between remote neurophysiological

events. There has been considerable methodological developments for quantifying functional connectivity, including seed-based approaches (Hampson et al., 2002) that compute correlations between a selected voxel (seed) and other voxels within the brain. Also, Patel et al. (2006a) and Patel et al. (2006b) develop a Bayesian modeling approach that quantifies functional connectivity as well as hierarchical relationships between functionally connected voxels, referred to as ascendancy.

Our model captures the functional connectivity between voxels within a defined anatomical region as well as inter-regional functional connectivity. A measure of the strength of the intra-regional functional connectivity is given by

$$\rho_{gj} = \frac{\gamma_{gg}^{(j)}}{\gamma_{gg}^{(j)} + \sigma_{gj}^2}. \quad (4)$$

Thus, ρ_{gj} reflects the coherence or the similarity in neural activity between voxels within a given anatomical structure and may vary for different effects, e.g. for patients and controls and for baseline versus post-treatment measurement occasions. One may structure the model to address intra-regional correlations within the same hemisphere or employ an extended model to additionally capture bilateral intra-regional correlations between voxels in separate hemispheres, e.g. the right and left amygdala.

Another component of the functional connectivity is that which occurs between anatomical regions, captured in our framework by modeling $\alpha_{ij} = (\alpha_{i1j}, \dots, \alpha_{iGj})'$ as

$$\alpha_{ij} | \Gamma_j \sim N(\mathbf{0}, \Gamma_j)$$

We specify a Wishart prior for Γ_j^{-1} , allowing a flexible unstructured covariance matrix for the α_{ij} . The multivariate structure enables us to compute the inter-regional functional connectivity matrix (with respect to stimulus j) by

$$\mathbf{R}_j = \{\text{Diag}(\Gamma_j)\}^{-1/2} \Gamma_j \{\text{Diag}(\Gamma_j)\}^{-1/2}, \quad (5)$$

where the (g_1, g_2) element in \mathbf{R}_j represents the functional connectivity between anatomical regions g_1 and g_2 .

3.4 Prior specifications

To effect our Bayesian hierarchical model, we set $a_0 = 0.1$, $b_0 = 0.005$, $c_0 = 0.1$, $d_0 = 0.01$, and $h_0 = G$. These values were evaluated to ensure that they resulted in a diffuse enough prior so that results were governed by the observed data. The selection for h_0 establishes a diffuse prior for the covariance matrix, without raising concerns about an improper posterior distribution. We empirically specify μ_{0gj} by calculating the global mean across all subjects and intra-regional voxels.

For the inverse-Wishart prior, the degrees of freedom must satisfy $h_0 \geq G$ to yield a proper prior distribution. The spatial prior for α_{ij} becomes non-informative as h_0 approaches 0 (West and Harrison, 1989), so we set $h_0 = G$ to reflect the most diffuse prior that our data can support, while employing a proper prior distribution. A seemingly natural choice for \mathbf{H}_{0j} is a point estimate of Γ_j . We use the sample covariance matrix corresponding to the j th effect to obtain \mathbf{H}_{0j} , calculated from the subject- and effect-specific mean activity levels in each of the anatomical regions. Note that according to our model, the use of the sample covariance matrix provides a conservative estimate of the true variation as follows. Given our hierarchical model, the variance-covariance matrix of $\bar{\beta}_{ij} = (\bar{\beta}_{i1j}, \dots, \bar{\beta}_{iGj})'$, where $\bar{\beta}_{igj} = \frac{1}{V_g} \sum_{v=1}^{V_g} \beta_{igj}(v)$, has additive contributions from Γ_j and $\text{diag}(\sigma_{1j}^2/V_1, \dots, \sigma_{Gj}^2/V_G)$. However, we specify a prior based on a matrix \mathbf{H}_{0j} that subsumes both components of variation. We favor this use of a conservative point estimate, to safeguard against under-estimating the variability. In addition to specifying a diffuse prior and using a conservative estimate, we examine the sensitivity of our results to the sample covariance matrix by artificially reducing the correlations (covariances) using

$$\mathbf{H}_{0j}^* = (1 - \omega)\mathbf{H}_{0j} + \omega \{\text{diag}(\mathbf{H}_{0j})\}.$$

where $0 \leq \omega \leq 1$. To avoid introducing prior information that does not seem physiologically plausible and that is not supported by the data, we consider small to moderate departures from the sample covariance matrix in our sensitivity analyses. For example, we consider $\omega \in [0, 0.25]$, reflecting up to a 25% decrease in the correlation estimates produced by our data.

4 Estimation and posterior inference

We implement MCMC methods for estimation using Gibbs sampling. Applying MCMC methods in our context is complicated by the massive amount of data, the vast number of spatial locations, and the large number of parameters. While our model maps well to characteristics of functional neuroimaging data and is neurophysiologically plausible, the conjugate model specification facilitates estimation by providing substantial reductions in computing time and memory.

We draw simulations from the joint posterior distribution by applying Gibbs sampler to the associated full conditional distributions. To simplify our presentation of the full conditional distributions, let $\mathbf{D}_j^{-1} = \text{diag}(V_1\sigma_{1j}^{-2}, \dots, V_G\sigma_{Gj}^{-2})$, $\bar{\boldsymbol{\beta}}_{gj} = \frac{1}{K_j} \sum_{v=1}^{K_j} \boldsymbol{\beta}_{igj}$, $\bar{\boldsymbol{\mu}} = (\bar{\mu}_1, \dots, \bar{\mu}_{Gj})'$, with $\bar{\mu}_{gj} = \frac{1}{V_g} \sum_{v=1}^{V_g} \mu_{gj}(v)$, and $u_{igj} = (\boldsymbol{\beta}_{igj} - \boldsymbol{\mu}_{gj} - \mathbf{1}\alpha_{igj})'(\boldsymbol{\beta}_{igj} - \boldsymbol{\mu}_{gj} - \mathbf{1}\alpha_{igj})$. The full conditionals are given by the following:

$$\begin{aligned}
 \boldsymbol{\mu}_{gj} &\sim \text{Normal} \left[\boldsymbol{\Omega}_{gj} \left\{ \lambda_{gj}^{-2} \mu_{0gj} + K_j \sigma_{gj}^{-2} (\bar{\boldsymbol{\beta}}_{gj} - \mathbf{1}\bar{\boldsymbol{\alpha}}_{gj}) \right\}, \boldsymbol{\Omega}_{gj} \right] \\
 \sigma_{gj}^{-2} &\sim \text{Gamma} \left\{ a_0 + K_j V_g / 2, \left(\frac{1}{b_0} + \frac{1}{2} \sum_{i=1}^{K_j} u_{igj} \right)^{-1} \right\} \\
 \boldsymbol{\alpha}_{ij} &\sim \text{Normal} \left[\boldsymbol{\Psi}_j \left\{ \mathbf{D}_j^{-1} (\bar{\boldsymbol{\beta}}_{ij} - \bar{\boldsymbol{\mu}}_j) \right\}, \boldsymbol{\Psi}_j \right] \\
 \lambda_{gj}^{-2} &\sim \text{Gamma} \left\{ c_0 + V_g / 2, \left(\frac{1}{d_0} + \frac{(\boldsymbol{\mu}_{gj} - \boldsymbol{\mu}_{0gj})'(\boldsymbol{\mu}_{gj} - \boldsymbol{\mu}_{0gj})}{2} \right)^{-1} \right\} \\
 \boldsymbol{\Gamma}_j^{-1} &\sim \text{Wishart} \left\{ \left(h_0 \mathbf{H}_0 + \sum_{i=1}^{K_j} \boldsymbol{\alpha}_{ij} \boldsymbol{\alpha}_{ij}' \right)^{-1}, h_0 + K_j \right\},
 \end{aligned} \tag{6}$$

where $\boldsymbol{\Omega}_{gj} = (\lambda_{gj}^{-2} + K_j \sigma_{gj}^{-2})^{-1} \mathbf{I}$ and $\boldsymbol{\Psi}_j = (\boldsymbol{\Gamma}_j^{-1} + \mathbf{D}_j^{-1})^{-1}$.

A key advantage of our Bayesian modeling framework, relative to prior approaches employing classical statistical methods, is that we obtain samples from the joint posterior distribution for all of the model parameters. A related advantage is that we can easily estimate functions of the model parameters using the posterior samples. Obtaining posterior samples for all parameters and relevant functions of the model parameters facilitates inferences by allowing us to formulate associated probability statements and to compute MCMC-based credible intervals, giving a specified probability that the parameter of interest lies in a particular interval. In addition to the parameters in model (2), we will estimate ρ_g to quantify intra-regional functional connectivity, \mathbf{R}_j for inter-

regional connectivity, and θ_{gj} for regional-level effects, e.g. comparing pre- and post-treatment brain activity levels in specified anatomical regions.

5 Results

We apply our Bayesian hierarchical model to both the fMRI study of inhibitory control in cocaine-dependent men as well as to the auditory memory encoding and retrieval study of individuals who are at high risk for developing Alzheimer's disease.

5.1 Voxel-level activations

Cocaine dependence data

Our analysis provides voxel-specific probabilities of any event that is definable as a function of the model parameters, providing a flexible framework to make inferences pertaining to a range of study objectives. We focus on inferences about neural processing alterations related to inhibitory control for cocaine-dependent men before and after intensive behavioral therapy for their addiction. To adjust for learning (or other) effects associated with repeated scanning at baseline and at the follow-up period, we quantify treatment-emergent changes in measured brain activity in the cocaine addicts relative to the corresponding alterations in the healthy control subjects. In summarizing the results from our analysis of the inhibitory control data, we quantify treatment-related changes in brain activity as the post-treatment quantity of interest (e.g. group average within a voxel or within a region) minus the pre-treatment quantity. Similarly, we quantify changes for the control subjects as follow-up estimates minus the baseline estimates.

Figure 1 displays axial slices showing voxels exhibiting treatment-emergent inhibitory control-related changes in neural processing for the cocaine-dependent men that exceed the corresponding changes in the controls. The highlighted voxels have posterior probabilities exceeding 0.70 and include the medial orbital frontal cortex (BA 11), the left thalamus and left middle frontal gyrus (BA 46), the left and right middle frontal gyrus (BA 9), and the cingulate gyrus (BA 31, 32). The voxel-specific effects of treatment indicate the recruitment of thalamo-cortical pathways in attaining the relapse prevention goals of behavioral therapies. Functional inferences include the involvement of

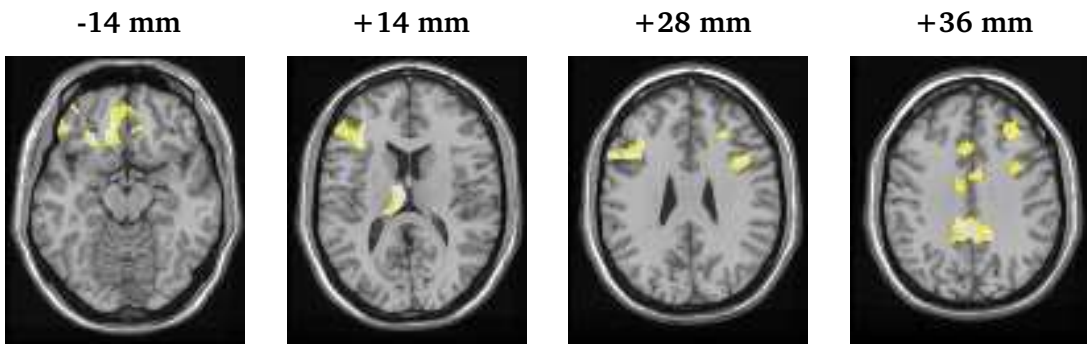


Figure 1: Maps of voxel-specific treatment-emergent activations for the cocaine-dependent subjects, adjusted for the corresponding baseline-to-follow-up changes in the control subjects. The maps portray voxel-specific posterior probabilities, exceeding 0.70, of increased activity from baseline to the post-treatment period for the cocaine addicts, relative to (minus) the corresponding difference in the control subjects. The axial slices are at various distances (in millimeters (mm)) from the anterior-posterior commissural plane. The activations include the medial orbital frontal cortex (BA 11) [at -14 mm], the left middle frontal gyrus (BA 46) and left thalamus [at $+14$ mm], bilaterally in the middle frontal gyrus (BA 9) [at $+28$ mm], and along the cingulate gyrus (BA 31, 32), with the posterior cingulate activation appearing most spatially extensive [at $+36$].

alterations in drug valuation and in the mental representation of drug contingencies, facilitation of regulatory control of responses to drug incentives, and the engagement of cognitive control processes related to response conflict monitoring drug availability.

Alzheimer's disease data

The Alzheimer's disease data showed no significant areas of voxel-level activation differences between groups. Specifically, in no regions did at-risk subjects present evidence of significantly higher or lower activation than controls. The areas that survived thresholds were diffuse and not localized, which mirrors results found using standard voxel-level techniques. This may in part be due to the finer decomposition of imaging area into small regions of interest used in this analysis. As shown below, there was more support for the association of Alzheimer's risk with alterations in regional activations and differences in connectivity.

5.2 Regional activations and functional connectivity

In addition to voxel-level inferences, our model provides a framework for investigating (de)activations at a regional level. Regional-level analyses have the advantage that they may pool strength from voxels across the entire region to reveal task-induced alterations in neural processing, even when the voxel-specific analyses do not reveal such changes. However, it is important to note that, depending on the number of activated voxels in a region and the magnitudes of these activations, one may not detect regional increases (decreases) in activity, despite having voxels within the region that show elevated (decreased) activity.

Cocaine dependence data

We evaluate regional treatment-related differences in the neural response to the inhibitory control task by computing mean estimates of the post-treatment period minus the pre-treatment period for the cocaine-dependent subjects, relative to the corresponding estimate in the control subjects. Specifically, we obtain probabilities that the treatment response in the cocaine addicts exceeds the (learning) response in the control group, and similarly we quantify the likelihood that the learning response in the controls exceeds the treatment-emergent response for the addicts.

Figure 2 displays regions for which the posterior probabilities of treatment-related brain activity changes in the cocaine-dependent subjects are greater than (green) and less than (blue) than the changes in the healthy control subjects. The data provide evidence of treatment-related increases in inhibitory control-related activity in the medial orbital frontal cortex and the gyrus rectus, with posterior probabilities of 0.85 and 0.94, respectively, estimated from the posterior distribution samples. Examining the posterior mean estimates for the baseline to follow-up changes in brain activity separately for each group, we observe that the cocaine-dependent subjects exhibit an increase in activity in the medial orbital frontal cortex following treatment, whereas the control subjects show little change. The cocaine addicts also reveal large increases in activity following treatment in the gyrus rectus (0.79) compared to a slight increase in the controls (0.02). Our findings indicate that there is an estimated 85% chance that the change in neural functioning in the medial orbital frontal cortex from pre- to post-treatment exceeds the corresponding change in the control subjects, and

similarly there is an estimated 94% chance that the treatment response in the gyrus rectus outpaces the learning response in the controls.

Our analysis also determines that the right inferior parietal cortex (posterior probability (pp)=0.89), the right hippocampus (pp=0.95), and the left inferior orbital frontal cortex (pp=0.95) all show greater baseline to follow-up changes in neural processing for the controls than pre- to post-treatment changes in the cocaine addicts. Both the cocaine addicts and the healthy controls show decreased activity in the right inferior parietal cortex at follow-up, on average, so one may view our results as indicating an 89% chance that the decrease in the cocaine addicts is more extensive than the decrease in the controls. In the right hippocampus and in the left lateral orbital frontal cortex, the cocaine addicts demonstrate a decrease in activity following treatment, while the controls reveal increased activity. Therefore, our results indicate an estimated 95% chance that the baseline to follow-up change in the regional mean BOLD response is greater in the controls than it is in the cocaine-dependent subjects. The results of the region-level analysis suggests the engagement of behavioral regulatory functions related to treatment-emergent activation of the ventromedial pre-frontal cortex and the lesser demand for the attentional, habit suppression and memory retrieval processes necessary to foregoing cocaine use in early abstinence states.

Our model yields estimates of the within-region correlations, based on the posterior means of ρ_{gj} , giving a measure of regional coherence or intra-regional functional connectivity (see Table 1). We obtain separate estimates of the regional coherence for the cocaine addicts before and after treatment as well as for the control subjects at baseline and at follow-up. Both groups of subjects exhibit more synchronized intra-regional neural processing during the follow-up session relative to baseline, revealed by the increases in intra-regional correlations for each anatomical region. The cocaine addicts show a fair degree of coherence following treatment between voxels comprising the left thalamus (0.55), the right inferior parietal lobule (0.50), the gyrus rectus (0.51), and the medial orbital frontal cortex (0.49). The control subjects exhibit the strongest intra-regional correlations at the follow-up assessment in the medial (0.53) and right lateral (0.50) portions of the orbital frontal cortex.

We also evaluate whether the data provide evidence of more synchronous intra-regional neural functioning at follow-up relative to baseline by considering the ratio of the pre-treatment (or

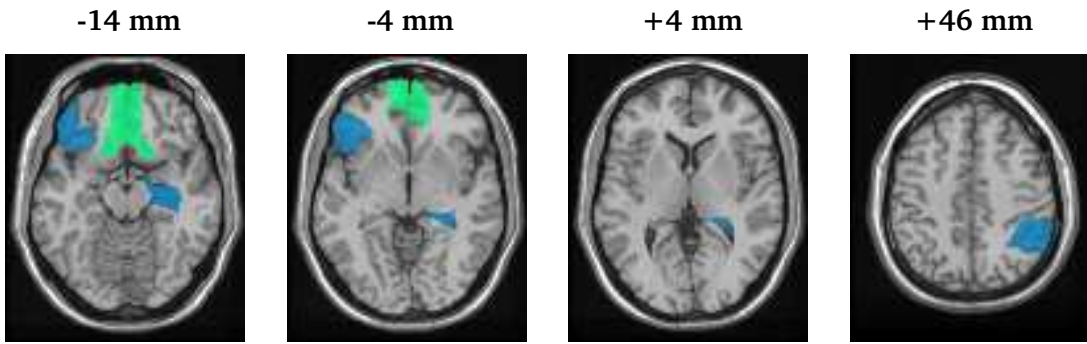


Figure 2: Map of regional treatment-emergent activations (green) and deactivations (blue) for the cocaine-dependent subjects, adjusted for the corresponding baseline-to-follow-up changes in the control subjects. The axial slices portray regional (de)activations at various distances (in millimeters) from the anterior/posterior commissural plane. All regions displayed have posterior probabilities of (de)activation exceeding 0.80. The deactivations include the right inferior parietal cortex (at +46 mm), the right hippocampus (at -4 and +4 mm), and the left lateral orbital frontal cortex (at -4 and -14 mm). The maps reveal evidence for activation in the right and left medial orbital frontal cortex (at -4 and -14 mm) as well as the right and left gyrus rectus (at -14 mm).

baseline) correlation to the post-treatment (or follow-up) correlation for each region, say ρ_{g1}/ρ_{g2} (see Table 1). A value of this ratio falling below one indicates greater intra-regional coherence at follow-up, relative to baseline. The strongest evidence for more synchronous intra-regional neural functioning at the follow-up session exists for the cocaine addicts, with the upper bounds of the MCMC-based 90% credible intervals for ρ_1/ρ_2 falling below one for the right middle frontal gyrus, the right pars operculum of the inferior frontal cortex, the pars triangularis of the left inferior frontal cortex, the right lateral orbital frontal cortex, the gyrus rectus, and the right inferior parietal cortex, while all of the 90% credible intervals for the controls overlap one. These results suggest that a further description of treatment-related cocaine abstinence is the greater coherence of neural information processing in frontal and parietal brain regions involved in response inhibition.

| Region | Patients | | | Controls | | |
|----------------|----------|------|-------------|----------|------|-------------|
| | BL | FU | 90% CI | BL | FU | 90% CI |
| R Mid Fr | 0.00 | 0.42 | [0.00,0.48] | 0.01 | 0.23 | [0.01,8.89] |
| R Fr Inf Op | 0.01 | 0.47 | [0.01,0.87] | 0.04 | 0.36 | [0.06,6.69] |
| L Fr Inf Tri | 0.02 | 0.42 | [0.02,0.97] | 0.02 | 0.20 | [0.05,7.96] |
| L Inf OF | 0.02 | 0.31 | [0.03,2.50] | 0.02 | 0.31 | [0.03,5.04] |
| R Inf OF | 0.01 | 0.42 | [0.01,0.68] | 0.01 | 0.50 | [0.01,1.98] |
| R/L Med OF | 0.02 | 0.49 | [0.02,1.38] | 0.07 | 0.53 | [0.06,4.63] |
| R/L Rectus | 0.05 | 0.51 | [0.04,0.85] | 0.04 | 0.36 | [0.04,3.17] |
| R/L Mid Cing | 0.04 | 0.48 | [0.04,1.09] | 0.01 | 0.21 | [0.02,4.09] |
| R Hippo | 0.032 | 0.43 | [0.03,1.52] | 0.029 | 0.26 | [0.05,6.75] |
| R Inf Parietal | 0.00 | 0.50 | [0.00,0.54] | 0.03 | 0.45 | [0.03,3.15] |
| L Thal | 0.04 | 0.55 | [0.04,1.18] | 0.036 | 0.38 | [0.05,2.28] |

Table 1: Posterior median estimates of the intra-regional correlations (functional connectivity) for selected anatomically-defined brain regions. Separate estimates appear for patients and controls as well as for baseline and follow-up scanning sessions. The 90% credible intervals correspond to the ratio of the baseline regional correlation relative to the regional correlation during the follow-up period. (BL=Baseline, FU=Follow-up at 4 weeks, CI=credible interval, R=right, L=left, Inf=inferior, Fr=frontal, Mid=middle, OF=orbital frontal, Cing=cingulum, Hippo=hippocampus, Op=Operculum, Thal = Thalmus)

Alzheimer's disease data

A similar analysis on the regional mean parameters and intra-regional functional connectivity was performed on the Alzheimer's disease data. There were 46 total regions of interest, each having a relevant intersection with the imaging area. Though all 46 were considered, areas of the temporal and limbic lobes are of particular interest, having been indicated as having either increased or decreased encoding activity between at-risk subjects and controls in the first wave of the Alzheimer's data or being thought to be involved with the (verbal memory) paradigm. Note that, due to the larger number of subjects and smaller imaging area, this data set allowed for a finer decomposition

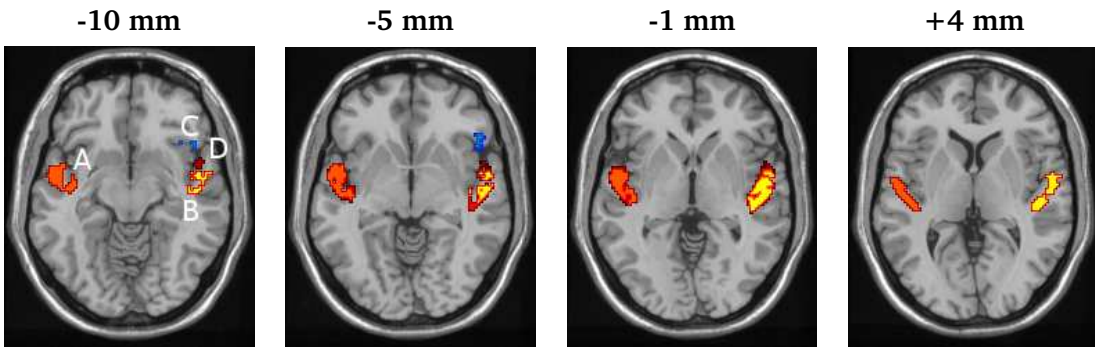


Figure 3: Map of regional activations and deactivations for subjects at risk for Alzheimer's disease relative to control subjects. The axial slices portray regional (de)activations at various distances (in millimeters) from the anterior-posterior commissural plane. All regions displayed have posterior probabilities of (de)activation exceeding 0.80. At risk had increased activation in the right superior temporal lobe (labeled A, orange), the left superior temporal lobe (labeled B, yellow), the left superior portion of the temporal pole (labeled, D, red), the orbital part of the right inferior frontal lobe (labeled C, blue).

of the regions of interest than the cocaine dependence data.

With regard to mean level activation, θ_{g1} was larger than θ_{g2} - i.e. controls had a higher estimated average activation in region g than at-risk subjects - in 92% of the simulations for the pars orbitalis of the left inferior frontal gyrus. In contrast, 90% and 94% of the simulations showed greater mean regional activity for the at-risk subjects in the left and right superior temporal gyri and the left superior portion of the temporal pole. However, in all four cases, the 95% (equi-tail) credible interval for the difference, $\theta_{g1} - \theta_{g2}$, overlapped zero.

Table 2 shows the estimates of intra-regional functional connectivity for all of the regions of interest, as well as confidence intervals for the ratio of at-risk to control subjects. Of note is the high amount of intra-regional connectivity suggested in the left and right mid temporal and left inferior (orbital) frontal cortex regions. As expected, however, these regions had few voxels. In general, there was a strong, linear negative trend between the number of voxels within a region and the estimated intra-regional functional connectivity, because smaller regions are likely to exhibit a greater degree of voxel correlation. It is difficult to assess to what extent the estimated correlations represent intrinsic factors, such as image resolution and preprocessing versus neu-

rophysiologic connectivity within the region. However, we emphasize that the images were not spatially smoothed as part of their preprocessing.

While decomposing the intra-regional connectivity into intrinsic imaging and processing factors and neurophysiologic connectivity is not possible, group-level differences in estimated intra-regional connectivity between control and at-risk subjects should reflect in actual differences in connectivity, since both groups were imaged on the same scanner and processed in the same way. The 95% credible intervals for the ratio of the correlations between the groups did not overlap one (indicating differential connectivity between groups) in the: left and right anterior cingulate gyrus (CIs of [0.52, 0.92] and [0.47, 0.84], respectively), the left mid cingulate gyrus ([0.53, 0.98]), the pars triangularis of the right inferior frontal cortex ([0.54, 0.96]), and the left superior frontal gyrus ([0.54, 0.92]). It is of interest to note that these regions were sites of differential activation patterns in the first wave of images for this study (Bassett et al., 2006). Also, controls showed significantly lower intra-regional functional connectivity than the at-risk subjects in these cases. This pattern was somewhat persistent; for example, 28 of the 46 posterior mean estimates of this correlation were larger for at-risk subjects. These findings suggest that at-risk subjects tend to have greater intra-regional connectivity than controls. This is consistent with the hypothesis that at-risk subjects are calling on greater neural processing reserves to perform the task.

5.3 Inter-regional Functional Connectivity

We examine the functional connectivity between anatomical regions by applying equation (5) to obtain an estimate of the correlation matrix from our posterior MCMC samples.

Cocaine dependence data

The correlation matrices, indexed by j , correspond to the cocaine addicts prior to treatment ($j = 1$), the cocaine addicts following treatment ($j = 2$), the control subjects at baseline ($j = 3$), and the controls at follow-up ($j = 4$). Figure 2 displays the correlation matrices corresponding to the respective posterior median covariance matrices obtained from the MCMC-based posterior samples, thresholded to retain correlations with magnitudes exceeding 0.4. To facilitate interpretation, we display positive correlations below the main diagonal and negative correlations above the main

diagonal of the correlation matrices, and naturally all of the diagonal elements equal one.

Our analysis suggests that treatment-related relapse prevention is associated with increased positive and negative connectivity within the inhibitory control network. Following treatment, the cocaine-dependent subjects exhibit positive functional connectivity between the right inferior frontal operculum and both the right lateral orbital frontal cortex (0.75) and the right inferior parietal cortex (0.92). Moreover, the right lateral orbital frontal cortex and the right inferior parietal cortex exhibit high correlations (0.75), revealing a three-way association between these nodes. The data also reveal functional connections between the right middle frontal gyrus and both the gyrus rectus (0.52) and the right hippocampus (0.58). We also identify functional connections between the left inferior frontal cortex (pars triangularis) and both the left thalamus (0.51) and right lateral orbital frontal cortex (0.51). Lastly, the gyrus rectus and the medial orbital frontal cortex exhibit functional connections during the inhibitory control task for the cocaine-dependent subjects, with an estimated correlation of 0.51. These results suggest that the relapse prevention goals of addiction therapy are encoded by enhanced synchronous activity in a neuronal network mediating the volitional control of habitual behaviors. Furthermore, the association of treatment-related cocaine abstinence with increased coincident activity in a neuronal network mediating extinction learning and memory retrieval suggests that relapse prevention is related to the extinction of prior learned drug contingencies.

Alzheimer's disease data

We also considered inter-regional functional connectivity in the Alzheimer's disease data set. Figure 5 shows the posterior means of the correlation matrices for both the control and at-risk subjects for the 46 regions of interest, thresholded at 0.4. Here, positive correlations are shown above and below the diagonal, as no negative correlations survived the threshold. As expected, the largest degree of inter-regional functional connectivity was found in bi-lateral regions. For example, among the controls there was a large posterior mean correlation between the left and right caudate (.62), the left and right medial portion of the cingulate gyrus (.67), the left and right middle frontal gyri (.61), and the left and right thalamus (.63). In addition, there was a large degree of connectivity, with several posterior mean correlations being above .5, within the frontal lobe subregions and cin-

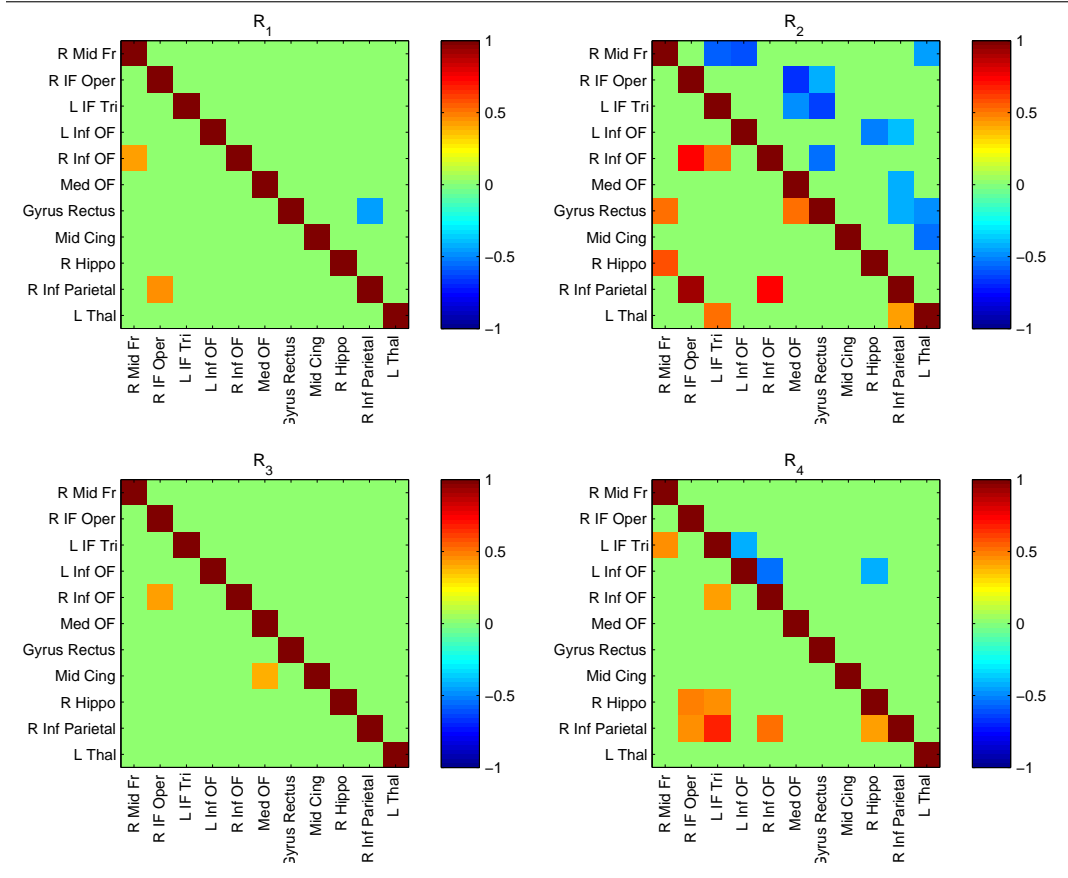


Figure 4: Posterior median estimates of inter-regional functional connectivity for cocaine addicts prior to treatment (R1) and following treatment (R2) and for control subjects at baseline (R3) and at follow-up (R4). The images are thresholded to remove all correlations with absolute values less than 0.4. In each image, positive correlations are shown below the main diagonal and negative correlations are shown above the diagonal.

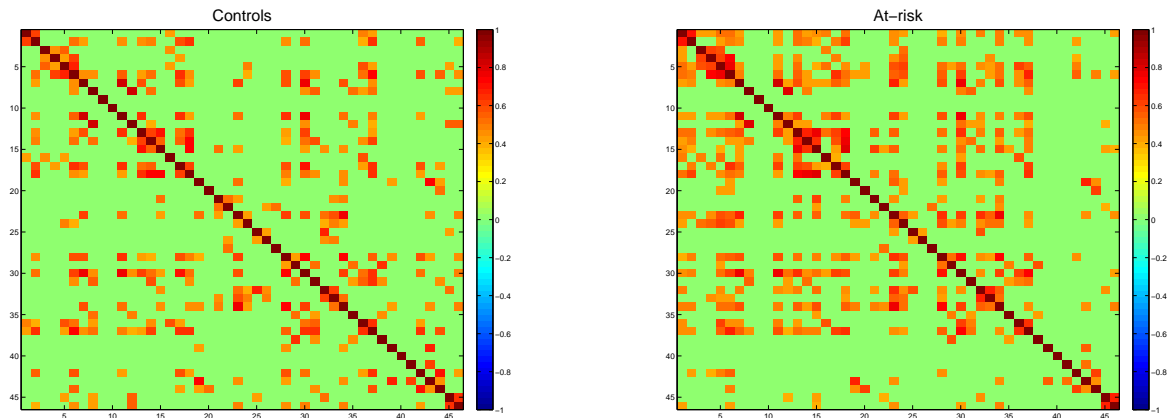


Figure 5: Posterior mean estimates of inter-regional functional connectivity for the Alzheimer’s disease data set. Corresponding region names and indices are given in Table 2.

gulate gyrus subregions. The at-risk subjects showed a higher degree of functional correlation, with correlations of .69, .77, .66 and .67 for the same regions, respectively. Of interest, the correlations within the frontal and cingulate gyri were also higher.

The most striking features of Figure 5 are the overwhelmingly positive correlations between the various regions and an overall pattern of much greater inter-regional functional connectivity among the at-risk group. This latter conclusion mirrors the result that at-risk subjects also showed a greater degree of intra-regional connectivity.

To formally compare the inter-regional functional connectivity between the two groups, two omnibus summaries of the variance matrices were used, the ratio of the determinants and greatest root statistic (see Mardia et al., 1979). The ratio of determinants had a 95% credible interval of [1.08, 109.55] while the greatest root statistic had a credible interval of [0.87, .91]. (The greatest root statistic is $1/2$ when the two variance matrices are equal.) Both intervals suggest a difference in inter-regional functional connectivity between the at-risk subjects and the controls. The investigations above suggest that there is, in general, a greater degree of inter-regional functional connectivity among the at-risk subjects. This is consistent with the hypotheses that subjects in the early stages of Alzheimer’s disease are calling on a greater amount of neuronal resources to perform the task demands.

5.4 Markov chain diagnostics

The volume of data in question prevents formal use of MCMC convergence tools, such as consistent batch means (Jones et al., 2006). Instead, more informal approaches were taken. Trace plots were used to assess convergence to stationarity for region-specific univariate parameters, such as σ_{gj} . Trace plots for voxel-specific parameters were investigated by taking a small random sample of voxels. All plots suggested rapid convergence to stationarity. For the reported region-level parameters, ad-hoc batch means methods, with batch sizes determined by informal investigation of the serial autocorrelation in the Markov chain were employed. Typical batch sizes were 100. A small number of burn-in samples (200) were used when starting values appeared to be in the extreme tails of the stationary density.

The impact of hyper-parameters on results was investigated first by comparing posterior mean estimates with corresponding moment-based estimates and secondly by sensitivity analysis performed by varying the prior parameters with regard to the degree of diffuseness. The impact of the Wishart prior specification was investigated as described in Section 3.4. Starting values were obtained using moment-based estimates. The choice of minimally informative gamma hyper-parameters was guided by comparing the gamma full conditionals to those obtained with the shape set to 0 and the scale set to ∞ .

6 Discussion

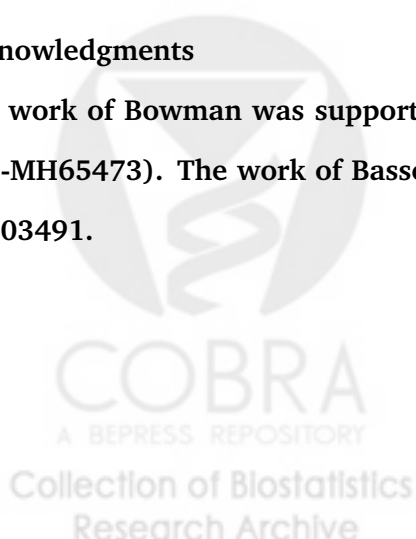
We propose a spatial Bayesian hierarchical model for analyzing functional neuroimaging data, which has several key advantages over alternative approaches. First, our model provides a unified framework to obtain neuroactivation inferences as well as functional connectivity inferences, rather than treating these as distinct analytical objectives. Secondly, we may investigate neuroactivation at both the voxel level and at a regional or VOI level. It is important to note that the voxel-level inferences provided by our approach account for prominent spatial correlations or functional connections in the brain, as detected by our Bayesian model. Similarly, the regional or VOI inferences account for spatial correlations in the data. Often, conducting a VOI analysis involves averaging the measured brain activity within the defined VOI, and then performing all subsequent

analyses as though the data represent a single location. Two drawbacks of this approach are that it risks oversimplifying effects in VOI's that do not exhibit relatively uniform activity throughout, e.g. failing to identify significant activity in a VOI that is partially active. Moreover, these analyses use variance estimates of the VOI-averages that assume independence between voxels, when we would rarely expect such an assumption to hold in practice. Our approach overcomes these two limitations because our model retains voxel-specific estimates of changes in measured brain activity to detect partially activated regions, and our model accounts for the correlations between the parameters involved in the regional summaries.

Additional advantages of our model stem from our use of a Bayesian paradigm, which here provides a range of flexible inferences. The Bayesian framework enables us to formulate probabilistic statements that help to quantify the evidence provided by our experimental data. The inference framework also allows us to compute credible intervals (or Bayesian confidence intervals) to make statistical inferences. Further, the MCMC estimation procedures produce samples from the joint posterior distribution of all of the model parameters, which facilitates estimation of and inferences about functions of the model parameters. In our fMRI examples, the intra-regional coherence (correlation) parameters served as particular examples that increased the interpretation content of our analyses. Despite the apparent complexity and rather rich formulation of our Bayesian hierarchical model as well as the high throughput nature of the data, computations for estimation are quite fast. For instance, estimation for the Bayesian hierarchical models for our two fMRI examples took less than 30 minutes each on a Linux cluster containing 4 processors with AMD Operton 850 CPUs (2.4Ghz) and 8GB RAM.

Acknowledgments

The work of Bowman was supported by the National Institute of Mental Health (NIH grant K25-MH65473). The work of Basset and Caffo was supported by NIH grants AG016324 and EB003491.



References

- Albert, P. and McShane, L. (1995). A generalized estimating equations approach for spatially correlated binary data: Applications to the analysis of neuroimaging data. *Biometrics*, 51:627–638.
- Aron, A. and Poldrack, R. (2006). Cortical and subcortical contributions to stop signal response inhibition: role of the subthalamic nucleus. *Journal of Neuroscience*, 26:2424–2433.
- Bassett, S., Yousem, D., Christinzio, C., Kusevic, I., Yassa, M., Caffo, B., and Zeger, S. (2006). Familiar risks for alzheimer's disease alters fMRI activation patterns. *Brain*, 129:1229–1239.
- Bookheimer, S., Strojwas, M., Cohen, M., Saunders, A., Pericak-Vance, M., Mazziotta, J., and Small, G. (2000). Patterns of brain Activation in people at risk for alzheimer's disease. *New England Journal of Medicine*, 343:450–456.
- Bowman, E. (2005). Spatiotemporal modeling of localized brain activity. *Biostatistics*, 6:558–575.
- Bowman, E. (2007). Spatio-temporal models for region of interest analyses of functional neuroimaging data. *Journal of the American Statistical Association*.
- Brookmeyer, R., Gray, S., and Kawas, C. (1998). Projections of Alzheimer's disease in the United States and the public health impact of delaying disease onset. *American Journal of Public Health*, 88:1337–1342.
- Friston, K., Frith, C., Liddle, P., and Frackowiak, R. (1993). Functional connectivity: the principal-component analysis of large (PET) data sets. *Journal of Cerebral Blood Flow and Metabolism*, 13:5–14.
- Friston, K., Holmes, A., Worsley, K., Poline, J., Frith, C., and Frackowiak, R. (1995). Statistical parametric maps in functional imaging: A general linear approach. *Human Brain Mapping*, 2(189–210).

Garey, L. (1994). *Brodmann's localisation in the cerebral cortex: the principles of comparative localisation based on cytoarchitectonics*. Springer, London. English translation of *Vergleichende Lokalisationslehre der Grosshirnrinde* by Korbinian Brodmann.

Gössl, C., Auer, D., and Fahrmeir, L. (2001). Bayesian spatiotemporal inference in functional magnetic resonance imaging. *Biometrics*, 57:554–562.

Hampson, M., Peterson, B., Skudlarski, P., Gatenby, J., and Gore, J. (2002). Detection of functional connectivity using temporal correlations in MR images. *Human Brain Mapping*, 15:247–262.

Holmes, A., Blair, R., G, W., and Ford, I. (1996). Nonparametric analysis of statistic images from functional mapping experiments. *Journal of Cerebral Blood Flow and Metabolism*, 16:7–22.

Jones, G., Haran, M., Caffo, B., and Neath, R. (2006). Fixed-width output analysis for Markov chain Monte Carlo. *Journal of the American Statistical Association*, 101:1537–1547.

Kalivas, P and Volkow, n. (2005). The neural basis of addiction: A pathology of motivation and choice. *American Journal of Psychiatry*.

Katanoda, K., Matsuda, Y., and Sugishita, M. (2002). Spatio-temporal regression model for the analysis of functional MRI data. *NeuroImage*, 17:1415–1428.

Mardia, K., Kent, J., and Bibby, J. (1979). *Multivariate Analysis*. Academic Press, San Diego.

Matsumoto, R., Nair, D LaPresto, E., Najm, I., Bingaman, W., Shibasaki, H., and Lüders, H. (2004). Functional connectivity in the human language system: a cortico-cortical evoked potential study. *Brain*, 127:2316–2330.

Patel, N., Bowman, F., and Rilling, J. (2006a). A bayesian approach to determining connectivity of the human brain. *Human Brain Mapping*, 27:267–276.

Patel, N., Bowman, F., and Rilling, J. (2006b). Determining hierarchical functional networks from auditory stimuli fMRI. *Human Brain Mapping*, 27:462–470.

- Penny, W., Trujillo-Barreto, N., and Friston, K. (2005). Bayesian fMRI time series analysis with spatial priors. *NeuroImage*, 24:350–362.
- Tariot, P. and Federoff, H. (2003). Current treatment for Alzheimer's disease and future prospects. *Alzheimer's disease and Associated Disorders*, 17:105–113.
- Tzourio-Mazoyer, N., Landeau, B., Papathanassiou, D., Crivello, F., Etard, O., Delcroix, N., Mazoyer, B., and M, J. (2002). Automated anatomical labeling of activations in SPM using a macroscopic anatomical parcellation of the MNI MRI single-subject brain. *NeuroImage*, 15:273–289.
- West, M. and Harrison, J. (1989). *Applied Bayesian forecasting and time series analysis*. Chapman and Hall / CRC, Boca Raton.
- Woolrich, M., Behrens, T., and Smith, S. (2004a). Constrained linear basis sets for HRF modelling using variational Bayes. *NeuroImage*, 21:1748–1761.
- Woolrich, M., Jenkinson, M., Brady, J., and Smith, S. (2004b). Fully Bayesian spatio-temporal modeling of fMRI data. *IEEE Transactions on Medical Imaging*.
- Worsley, K. (1994). Local maxima and the expected Euler characteristic of excursion sets of χ^2 , F, and t fields. *Advances in Applied Probability*, 26:13–42.
- Worsley, K., Evans, A., Marrett, S., and Neelin, P. (1992). A three-dimensional statistical analysis for rCBF activation studies in the human brain. *Journal of Cerebral Blood Flow and Metabolism*, 12:900–918.
- Worsley, K., Evans, A., Strother, S., and Tyler, J. (1991). A linear spatial correlation model, with applicability to positron emission tomography. *Journal of the American Statistical Association*, 86:55–67.
- Worsley, K., Liao, C., Aston, J., Petre, V., Duncan, G., Moralese, F., and Evans, A. (2002). A general statistical analysis for fMRI data. *NeuroImage*, 15:1–15.

| | Region | Ctr | AR | CI | | Region | Ctr | AR | CI |
|----|--------------|------|------|-------------|----|------------|------|------|-------------|
| 1 | L Cau | 0.30 | 0.27 | [0.86,1.43] | 24 | R Insula | 0.13 | 0.17 | [0.58,1.08] |
| 2 | R Cau | 0.38 | 0.35 | [0.84,1.34] | 25 | L Pal | 0.34 | 0.34 | [0.77,1.26] |
| 3 | L A Cing | 0.18 | 0.26 | [0.52,0.92] | 26 | R Pal | 0.30 | 0.30 | [0.76,1.29] |
| 4 | R A Cing | 0.16 | 0.26 | [0.47,0.84] | 27 | R PHG | 0.61 | 0.60 | [0.87,1.18] |
| 5 | L Mid Cing | 0.16 | 0.22 | [0.53,0.98] | 28 | L Po | 0.32 | 0.36 | [0.68,1.11] |
| 6 | R Mid Cing | 0.20 | 0.26 | [0.59,1.04] | 29 | R Po | 0.25 | 0.27 | [0.72,1.23] |
| 7 | L Inf Op Fr | 0.22 | 0.27 | [0.61,1.07] | 30 | L Pr | 0.19 | 0.22 | [0.66,1.18] |
| 8 | R Inf Op Fr | 0.18 | 0.20 | [0.68,1.23] | 31 | R Pr | 0.19 | 0.15 | [0.95,1.75] |
| 9 | L Inf OF | 0.57 | 0.63 | [0.78,1.06] | 32 | L Put | 0.31 | 0.31 | [0.76,1.28] |
| 10 | R Inf OF | 0.37 | 0.41 | [0.72,1.12] | 33 | R Put | 0.31 | 0.29 | [0.84,1.40] |
| 11 | L Inf Tr Fr | 0.21 | 0.27 | [0.60,1.05] | 34 | L Rol Op | 0.25 | 0.27 | [0.72,1.24] |
| 12 | R Inf Tr Fr | 0.18 | 0.26 | [0.54,0.96] | 35 | R Rol Op | 0.18 | 0.19 | [0.70,1.27] |
| 13 | L Mid Fr | 0.17 | 0.20 | [0.65,1.17] | 36 | L SMA | 0.19 | 0.20 | [0.71,1.28] |
| 14 | R Mid Fr | 0.19 | 0.19 | [0.72,1.30] | 37 | R SMA | 0.25 | 0.26 | [0.73,1.24] |
| 15 | L Sup Fr | 0.23 | 0.33 | [0.54,0.92] | 38 | R SMG | 0.50 | 0.48 | [0.87,1.26] |
| 16 | L Sup Med Fr | 0.23 | 0.23 | [0.75,1.32] | 39 | L Mid Temp | 0.51 | 0.54 | [0.80,1.14] |
| 17 | R Sup Med Fr | 0.32 | 0.36 | [0.69,1.12] | 40 | R Mid Temp | 0.48 | 0.45 | [0.86,1.33] |
| 18 | R Sup Fr | 0.27 | 0.34 | [0.62,1.03] | 41 | L Sup TP | 0.35 | 0.36 | [0.77,1.23] |
| 19 | L He | 0.48 | 0.42 | [0.94,1.41] | 42 | R Sup TP | 0.50 | 0.45 | [0.91,1.33] |
| 20 | R He | 0.27 | 0.30 | [0.70,1.17] | 43 | L Sup Temp | 0.28 | 0.27 | [0.81,1.37] |
| 21 | L Hippo | 0.38 | 0.47 | [0.65,1.00] | 44 | R Sup temp | 0.23 | 0.18 | [0.94,1.69] |
| 22 | R Hippo | 0.40 | 0.38 | [0.85,1.33] | 45 | L Thal | 0.13 | 0.17 | [0.58,1.10] |
| 23 | L Insula | 0.20 | 0.21 | [0.71,1.28] | 46 | R Thal | 0.15 | 0.17 | [0.66,1.23] |

Table 2: Posterior mean and credible interval (CI) estimates of regional correlations for the 46 regions of interest considered in the Alzheimer's disease study. (Retaining labels from Table 1. Additional notation is as follows, Cr = Control, AR = At-risk, A = Anterior, Cau = Caudate, He = Heschl gyrus, Med = medial, Pal = Pallidum, Pc = Postcentral gyrus, PHG = Parahippocampal gyrus, Pr = precentral gyrus, Rol = Rolandic, SMA = Supplementary motor area, SMG = Supramarginal gyrus, Sup = Superior, Temp = Temporal gyrus, TP = Temporal pole, Tr = Triangular)